Analysis of centrifugal homogenization and its applications for emulsification & mechanical cell lysis

Singh, Kaustub; Gupta, Ankur; Buchner, Abel John; Ibis, Fatma; Pronk, Joachim W.; Tam, Daniel; Eral, Huseyin Burak

DOI
10.1016/j.jcis.2019.03.036

Publication date
2019

Document Version
Final published version

Published in
Journal of Colloid and Interface Science

Citation (APA)
Singh, K., Gupta, A., Buchner, A. J., Ibis, F., Pronk, J. W., Tam, D., & Eral, H. B. (2019). Analysis of centrifugal homogenization and its applications for emulsification & mechanical cell lysis. *Journal of Colloid and Interface Science*, *547*, 127-135. https://doi.org/10.1016/j.jcis.2019.03.036

Journal of Colloid and Interface Science 547 (2019) 127–135

Contents lists available at ScienceDirect

Journal of Colloid and Interface Science

journal homepage: www.elsevier.com/locate/jcis

Regular Article

Analysis of centrifugal homogenization and its applications for emulsification & mechanical cell lysis

Kaustub Singh [a], Ankur Gupta [b], Abel-John Buchner [a], Fatma Ibis [a], Joachim W. Pronk [c], Daniel Tam [a], Huseyin Burak Eral [a,d,*]

[a] Process & Energy Department, 3ME Faculty, TU Delft, Leeghwaterstraat 39, Delft, The Netherlands
[b] Department of Mechanical and Aerospace Engineering, Princeton University, NJ, USA
[c] Department of Bionanoscience, Faculty of Applied Sciences, TU Delft, Van der Maasweg 9, Delft, The Netherlands
[d] Van't Hoff Laboratory for Physical and Colloid Chemistry, Debye Institute, Utrecht University, Padualaan 8, 3584 CH Utrecht, The Netherlands

GRAPHICAL ABSTRACT

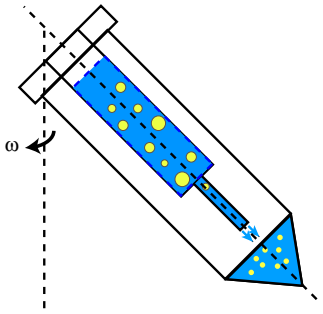

ARTICLE INFO

Article history:
Received 2 December 2018
Revised 9 March 2019
Accepted 11 March 2019
Available online 20 March 2019

MSC:
00-01
99-00

Keywords:
Centrifugal emulsification
Homogenizer
Centrifugation
Emulsions
Lysis

ABSTRACT

We detail the analysis of centrifugal homogenization process by a hydrodynamic model and the model-guided design of a low-cost centrifugal homogenizer. During operation, centrifugal force pushes a multiphase solution to be homogenized through a thin nozzle, consequently homogenizing its contents. We demonstrate and assess the homogenization of coarse emulsions into relatively monodisperse emulsions, as well as the application of centrifugal homogenization in the mechanical lysis of mpkCCD mouse kidney cells. To gain insight into the homogenization mechanism, we investigate the dependence of emulsion droplet size on geometrical parameters, centrifugal acceleration, and dispersed phase viscosity. Our experimental results are in qualitative agreement with models predicting the droplet size. Furthermore, they indicate that high shear rates kept constant throughout operation produce more monodisperse droplets. We show this ideal homogenization condition can be realized through hydrodynamic model-guided design minimizing transient effects inherent to centrifugal homogenization. Moreover, we achieved power densities comparable to commercial homogenizers by model guided optimization of homogenizer design and experimental conditions. Centrifugal homogenization using the proposed homogenizer design thus offers a low-cost alternative to existing technologies as it is constructed from off-the-shelf parts (Falcon tubes, syringe, needles) and used with a centrifuge, readily available in standard laboratory environment.

* Corresponding author.
E-mail address: H.B.Eral@tudelft.nl (H.B. Eral).
URL: http://www.erallab.com (H.B. Eral).

https://doi.org/10.1016/j.jcis.2019.03.036
0021-9797/

1. Introduction

Emulsification is an essential process in colloid and interface science [1]. Emulsions have been utilized as templates for self-assembly [2,3] and synthesis of tailored materials [4,5]. Emulsion stability is intimately related to droplet size distribution dictated by the preparation techniques i.e. details of the emulsification process (also known as homogenization) [6–8]. Consequently, a fundamental understanding of the process of homogenization and the mechanisms dictating the droplet size distribution will inform not only development of novel materials but also contribute to improving the stability of commonly used emulsions in industrial practice.

In a homogenizer, hydrodynamic shear forces break colloidal scale entities such as droplets, particles, and cells [9–15]. The pharmaceutical industry uses homogenizers to create micron-sized crystals to enhance dissolution rates of active pharmaceutical ingredients [16–18]. In the food industry, homogenizers are employed to create droplets that carry hydrophobic nutrients [19,20]. Additionally, homogenizers are used to create personal care products such as creams and lotions [21] even artificial blood cells [22]. The aforementioned applications often involve an emulsification step, *i.e.* breakup of oil droplets suspended in water or vice versa [7,23]. For emulsification, typical homogenizer designs include microfluidic homogenizers [24–26], high pressure homogenizers [14,27–30] and ultrasonic homogenizers [23,27,28]. Though these approaches excel at high-throughput applications (volume rates order liters per hour), they require high capital investment and are not designed to handle small volumes on the order of 1–10 mL.

Owing to their ability to manipulate small volumes, microfluidic homogenizers have attracted high levels of attention over the past two decades [31]. Microfluidic homogenization, utilizing micromanufactured structures such as barbs or nanowires, have been successfully demonstrated for emulsification and cell lysis [32–35]. Furthermore, microfluidic devices where the fluids are driven by centrifugal forces have shown promise in cell homogenization in lab-on-chip applications [36,37]. Such microfluidic platforms however usually require dedicated manufacturing equipment or trained personnel.

Centrifugal force has been utilized in combination with microstructured meshes and membranes to generate high shear for industrial homogenization applications [38]. Similar techniques have been exploited in synthesis of hydrogels [39–41], blood serum separation [42], and mixing of liquids in microfluidic channels [43,44]. Centrifugal force coupled with step emulsification in laminar flow conditions has also been used for digital droplet recombinase polymerase amplification [45,46] and producing high internal volume fraction emulsions [47]. However, a model guiding rational choice of experimental parameters across laminar and turbulent flow regimes has, to best of our knowledge, not previously been proposed. Therefore, we propose a hydrodynamic model and a simple experimental setup by eliminating the meshes and membrane, and instead simply forcing the mixture of oil, water, and surfactant through a thin nozzle. Guided by the proposed model, we detail the design of a low-cost centrifugal homogenization device (CHD) that is able to process volumes on the order of 1—10 mL while maintaining shear rates comparable to commercial homogenizers. The proposed CHD can be constructed using components (centrifuge, syringes and needle as nozzle) available in standard laboratories. Therefore, our design is, due to its simplicity and low cost, of potential use for the broader effort of developing low-tech solutions for developing world in the context of point-of-care diagnostics and low-cost global health solutions [48–52].

In this article, we first elucidate the working mechanism of centrifugal homogenization for emulsification though experiments and analytical modelling. Next, we detail the model-guided experimental design of the CHD. The influence of centrifugal speed, number of passes, dispersed phase viscosity and nozzle size on the droplet size distribution is studied. Moreover, we demonstrate utility of CHD for emulsification and mechanical cell lysis. The novelty of our study lies in the development of a hydrodynamic model providing a physical understanding of centrifugal homogenization. Guided by this model, we were able to account for transient effects inherent to centrifugation with important practical consequences for centrifugal homogenization, eg. time-dependent liquid column height and centrifugal speed. We explained the interplay of experimental parameters dictating the droplet size distribution, and consequently emulsion stability. Moreover, we reached power densities comparable to commercial homogenizers through the hydrodynamic model guided design, despite the use of only readily available and inexpensive lab supplies in its construction. We believe physical insights drawn from this study will guide future optimization of centrifugal homogenization applications.

2. Materials and methods

2.1. Assembly of the centrifugal homogenization device

The basic architecture of the CHD consists of a reservoir within which the pre-emulsion to be homogenized is stored, and a nozzle through which the emulsion is forced by way of centrifugation (Universal 320 R, Hettich lab technologies), as illustrated in Fig. 1a. Two versions of the CHD device were constructed and tested: one with a single-diameter reservoir (the "single-stage device"), and one with an extra, wider, reservoir section (the "double-stage device"). These two arrangements are shown schematically in Fig. 1b and c, wherein the flow direction is oriented downwards. Photographs of the assembled single and double CHDs are given in Supplementary Information. The reasoning behind the double stage design is explained in Section 3.

All parts used in the construction of the device are readily available in a standard laboratory. The single stage reservoir for the pre-emulsion is constructed from a 2 mL transparent plastic syringe purchased with VWR catalog number 613-1629. For the double stage device, a 20 mL plastic sample bottle serves as the second, wider, reservoir section, and is glued to the upper end of the syringe (see Fig. 1c and supplementary information).

The nozzle is made from a standard stainless steel fluid dispensing needle, purchased from Nordson. Gauges (G) 27, 30 & 32, with inner diameter $d_n = [108, 160, 210]$ μm, are tested. The length of these stainless steel needles is always $h_n = 1.4$ cm. The needles are attached to the syringe and are secured with a Luer lock connection.

The apparatus is inserted inside a standard 50 mL Falcon tube by drilling a hole in the cap of the tube that matches the outer diameter of the reservoir. The gap between the syringe and the Falcon tube is sealed by using Parafilm. The Falcon tube serves as a collector for the homogenized emulsions.

2.2. Experimental procedure for emulsification

First, we prepared a pre-emulsion my mixing silicone oil (Sigma Aldrich, CAS: 63148-62-9,99% purity) with a 0.01 % w/w aqueous sodium dodecyl sulfate (SDS) (Sigma Aldrich, CAS: 151-21-3,98% purity) solution using a magnetic stirrer for 5 min at 200 RPM. The composition of the pre-emulsions was kept constant at 1% w/w oil - aqueous solution. We found the pre-emulsion to contain polydisperse oil droplets with average droplet size on the order of hundreds of microns (Fig. 1d). Next, the pre-emulsion was placed in the syr-

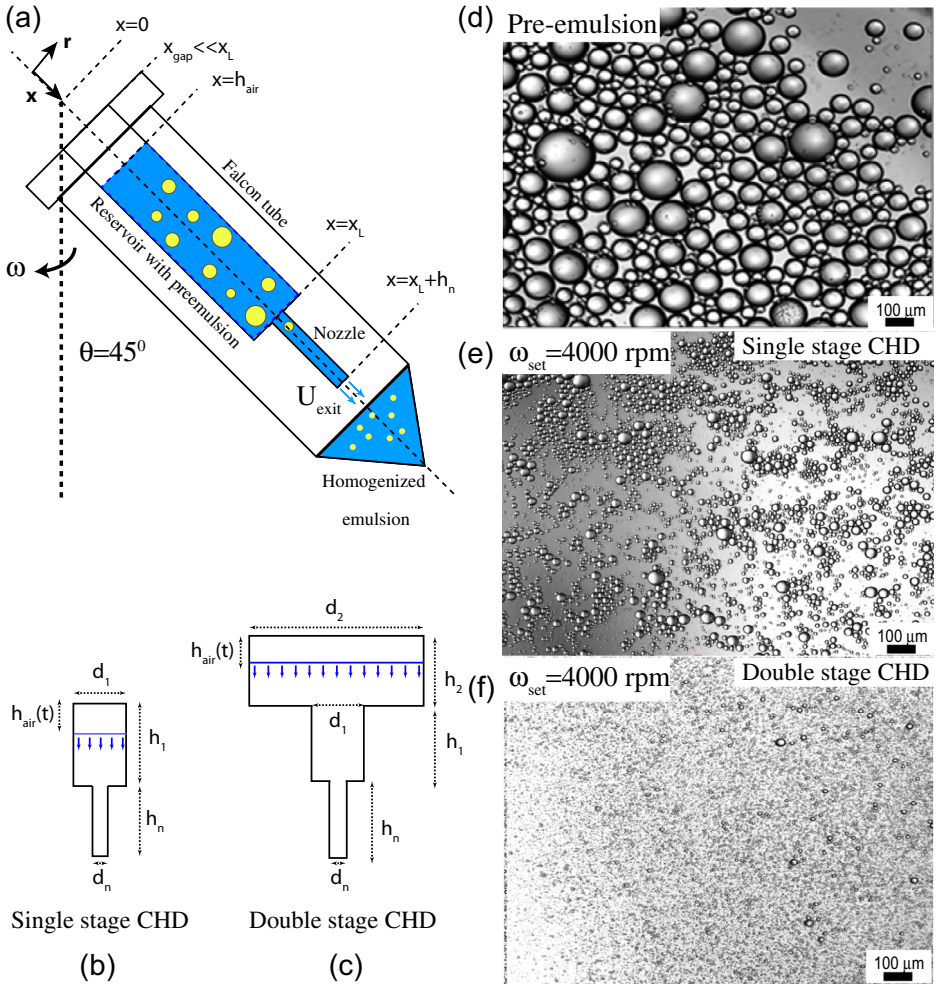

Fig. 1. (a) Illustration of the centrifugal homogenization device (CHD). A reservoir constructed of a 2 mL syringe (and plastic sample bottle in the double-stage case) is connected to a needle of diameter d_n and fitted inside a 50 mL Falcon tube through a hole drilled in the cap. The syringe is filled with oil (yellow)-in-water (blue) pre-emulsion. The device is positioned at an angle of $\theta = 45^\circ$ with the vertical axis of the centrifuge rotor. We define the coordinate along the axial direction of syringe and nozzle as x, and the perpendicular radial coordinate as r. Panels (b) & (c) illustrate the layout of the single and double stage CHDs, indicating the nomenclature used throughout this paper to refer to the CHD geometry. Since $x_{gap} \ll x_L, x_L \approx h_1$ for the single stage device and $x_L \approx h_1 + h_2$ for the double stage device. Panels (d), (e) & (f) are light microscopy images of the coarse pre-emulsion and the resulting emulsions after homogenization at 4000 RPM with 5 passes from single stage and double stage CHDs, respectively. (For interpretation of the references to colour in this figure legend, the reader is referred to the web version of this article.)

inge and forced through the needle by centrifugation at four different rotational speeds $\omega_{set} = [3000, 4000, 5000, 6000]$ RPM for 3 min. The centrifugation breaks the big droplets to create smaller sized emulsions. The centrifugation step was repeated 5 times at each rotational speed, *i.e.* the solution was passed through the nozzle 5 times. Unless otherwise stated, the number of passes was always equal to 5. The resulting emulsion was imaged under bright field using an inverted microscope (Nikon TE) equipped with a 20× objective (Fig. 1d–f). We varied the needle size as $d_n = [108, 160, 210]$ μm, and the oil viscosity $\mu_d = [5, 350, 1000]$ cP. All experiments were repeated 3 times, and an average value is reported here. The microscopy images were analyzed with commercial software Matlab using its circle-finder routine following a thresholding and binarization step. We have also explored the possibility of eliminating the premixing step. Without the premixing step, the homogenization process still took place yet more disperse droplet size distributions were observed at 4000 rpm.

2.3. Experimental procedure for cell lysis

A total of 24 flasks (T75, 75 cm^2 surface area) of mpkCCD [53] mouse kidney cell culture were grown in DMEM/F-12 Glutamax medium (Gibco) supplemented with ITS-G (Gibco), Dexamethasone (Sigma Aldrich), Triiodotyrine (Sigma Aldrich), Epidermal growth Factor (EGF; Sigma Aldrich), HEPES buffer (Gibco), Fetal Calf Serum (FCS; Gibco) and Penicillin/Streptomycin (Gibco) for 7 days until $> 90\%$ confluence. All chemicals are Mammalian Cell Culture applications purity. Each flask contained 10 mL of growth medium. Cells were then trypsinized to detach the cells from the flask surface. After cells were detached, trypsinization was inhibited by addition of 9 mL cell medium. Cell cultures were then pooled and pelleted by centrifugation for 15 min, 1000*g*, at 4 °C. Pelleted cells were re-suspended in medium to a total volume of 90 mL, yielding a culture with concentration 1.3×10^6 cells/mL. Cells were counted using a cell counting chamber (Marienfield) and cell viability ($> 99\%$) was checked by trypan-blue staining. The culture was refrigerated at 4 °C to prevent further growth.

Volumes of the cell culture of 10 mL were placed in the CHD and extruded at $\omega_{set} = 3000, 6000$, or 9000 RPM for two minutes. The resulting homogenized culture was then re-introduced into the centrifugal homogenization device and the process repeated ten times.

3. Design evolution of the centrifugal homogenization device

We first focus on the evolution of our design from a single stage to a double stage CHD, informed by a theoretical analysis of the

factors pertinent to effective homogenization. For optimum performance, the exit velocity of the mixture from the nozzle should be large and relatively constant with time. However, since the height of the liquid column in the syringe changes with time, the exit velocity from the nozzle varies, which is detrimental to the performance of CHD, possibly increasing the polydispersity of the resulting emulsion. Furthermore, the rotational speed ω increases with time and then attains a constant value equal to the specified value ω_{set} (see Fig. 2a). The time-dependent behavior of ω also leads to a non-uniform shear rate, as explained later.

To quantify the aforementioned effects, we model the nozzle, syringe, and additional reservoir as cylindrical pipes with diameters d_n, d_1 and d_2 respectively (Fig. 1b and c). We denote the length of the nozzle as h_n, length of the syringe as h_1, and length of additional reservoir as h_2. We assume that for the single stage device the volume of liquid inside the nozzle is negligible compared to the amount of liquid inside the syringe. We denote the height of the air column in the syringe as $h_{air}(t)$. Similarly, for the double stage device, we assume that the volume of liquid inside the nozzle and syringe is negligible compared to the volume of liquid inside reservoir. Here, the height of the air column in the reservoir is denoted as $h_{air}(t)$. We also assume that the viscosity and density of the mixture are given by the continuous phase density ρ_c and viscosity μ_c, and U_{exit} is the exit velocity from the nozzle. Further, we assume that the flow velocity inside the syringe and the reservoir is negligible as compared to the flow velocity inside the nozzle. We also assume that the velocity is unidirectional and is parallel to the axial direction of the nozzle. We neglect the effect of gravity and assume that the flow is quasi-steady and incompressible.

First, we focus on the single stage device. We define the coordinate along the length of the tubes as x and radial coordinate as r; see Fig. 1(a). Since $x_{gap} \ll x_L$, we approximate $x_L \approx h_1$. Assuming the flow is laminar, invoking the equation of continuity, utilizing that the velocity u in the syringe is negligible and u is unidirectional inside the nozzle, we write the momentum conservation in a rotating frame of reference as

$$\frac{dP}{dx} = \begin{cases} \frac{\rho_c \omega^2 \sin^2\theta}{2} x & h_{air} \leqslant x \leqslant x_L, \\ \frac{\mu_c}{r}\frac{d}{dr}\left(r\frac{du}{dr}\right) + \frac{\rho_c \omega^2 \sin^2\theta}{2} x & x_L \leqslant x \leqslant x_L + h_n, \end{cases} \tag{1a}$$

where P is the pressure. By integrating Eq. (1a) with boundary conditions $P(x = h_{air}) = P_{atm}$ and $P(x = x_L + h_n) = P_{atm}$, and ensuring that pressure is equal at $x = x_L$, we obtain

$$\frac{\mu_c}{r}\frac{d}{dr}\left(r\frac{du}{dr}\right) = -\frac{\rho_c \omega^2 \sin^2\theta}{2}\left(\frac{(x_L + h_n)^2 - h_{air}^2}{h_n}\right) = -\frac{|\Delta P|}{h_n}, \tag{1b}$$

where $|\Delta P|$ is the effective pressure drop across the nozzle as given by Eq. (1b). Eq. (1b) demonstrates that the single stage device can be treated as a circular pipe with an effective $|\Delta P|$. In the remaining derivation, we write $x_L \approx h_1$. Therefore, utilizing the relations for circular pipe (for both laminar and turbulent flows), we obtain

$$\frac{dh_{air}}{dt} = \frac{d_n^2}{d_1^2} U_{exit}, \tag{2a}$$

$$|\Delta P| = \rho_c \frac{\omega^2 \sin^2\theta}{2}\left((h_1 + h_n)^2 - h_{air}^2\right), \tag{2b}$$

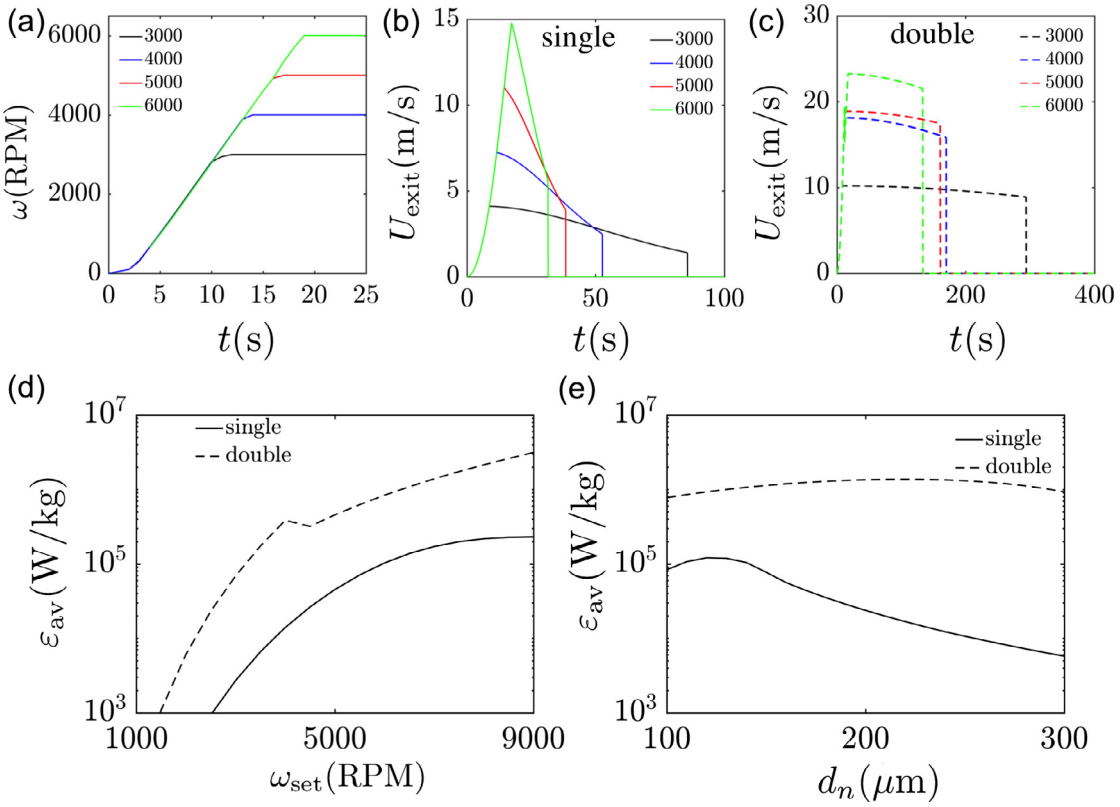

Fig. 2. Evolution of the CHD design from single stage to double stage. (a) Measured rotational speeds $\omega(t)$ for different set values ω_{set}. (b) Computed exit velocity U_{exit} from the nozzle for a single stage device for varying ω_{set} as given by Eq. (4) and (c) U_{exit} from a double stage device for varying ω_{set}, again calculated using (4) but where the emulsion height has been redefined as $H = h_n + h_1 + h_2$ and the wider diameter of the double-stage reservoir has been accounted for by replacing d_1 with d_2. d_n is here equal to 108 μm. Variation of ε_{av} for both devices with (d) ω_{set} (for $d_n = 108$ μm) and (e) d_n (for $\omega_{set} = 6000$ RPM), as given by Eq. (6). In these calculations, other parameters are held constant as: $h_n = 1.4$ cm, $h_1 = 6.6$ cm, $h_2 = 4.6$ cm, $\rho_c = 100$ kg/m^3, $\mu_c = 10^{-3}$ Pa·s.

$$|\Delta P| = \frac{2f\rho_c U_{\text{exit}}^2 h_n}{d_n}, \tag{2c}$$

$$f = \begin{cases} \frac{16}{\text{Re}}, & \text{Re} \leqslant 2100, \\ 0.079\text{Re}^{-1/4}, & \text{Re} > 2100, \end{cases} \tag{2d}$$

where $\text{Re} = \frac{\rho_c U_{\text{exit}} d_n}{\mu_c}$, f is a friction factor, and the angle θ is as defined in Fig. 1a. Based on the experimental results shown in Fig. 2a, we approximate $\omega(t)$ as

$$\omega(t) = \begin{cases} \dot{\omega} t & t \leqslant \dot{\omega}^{-1}\omega_{\text{set}}, \\ \omega_{\text{set}} & t \geqslant \dot{\omega}^{-1}\omega_{\text{set}}. \end{cases} \tag{3}$$

To simplify calculations, we define $H = h_n + h_1$ and combine Eqs. ((2a)–(2c)), to get

$$\frac{dh_{\text{air}}}{dt} = \begin{cases} U_0 \frac{d_n^2}{d_1^2} \frac{\omega^2}{\omega_{\text{set}}^2}\left(1 - \frac{h_{\text{air}}^2}{H^2}\right) & \text{Re} \leqslant 2100 \\ U_0 \frac{d_n^2}{d_1^2}\left(\frac{\omega^2}{\omega_{\text{set}}^2}\left(1 - \frac{h_{\text{air}}^2}{H^2}\right)\right)^{4/7} & Re > 2100 \end{cases} \tag{4a}$$

$$U_0 = \begin{cases} \frac{\rho_c \omega_{\text{set}}^2 d_n^2 H^2 \sin^2\theta}{64\mu_c h_n} & \text{Re} \leqslant 2100 \\ 1.93\left(\frac{\rho_c d_n^5 \omega_{\text{set}}^8 H^8 \sin^8\theta}{\mu_c h_n^4}\right)^{1/7} & Re > 2100 \end{cases} \tag{4b}$$

where $h_{\text{air}}(0) = 0$ and U_0 is the maximum exit velocity from the nozzle. Numerical integration of Eqs. (4), gives the solution of $h_{\text{air}}(t)$, and we evaluate U_{exit} by using Eq. (2a) and (4a). During numerical integration, we only integrate up until the moment the syringe is completely emptied, $0 \leqslant t \leqslant t_f$, such that $h_{\text{air}}(t_f) = h_1$. This condition ensures that we integrate until all the liquid inside the syringe has been homogenized.

We plot the results for U_{exit} as a function of time for typical experimental conditions and different rotation rates ω_{set} (see Fig. 2b). The plot shows that U_{exit} varies with time, increasing to a maximum value, and reducing afterwards. Our results demonstrate that a larger ω_{set} increases the peak magnitude of U_{exit}. However, the increase in ω_{set} also leads to a more rapid decline in U_{exit}. Physically, increasing ω_{set} increases the driving force which increases U_{exit}. However, this also results in a faster decay in the height of liquid inside the homogenizer, leading to a faster decay in U_{exit}. Overall, since the volume of the liquid homogenized is constant irrespective of change in ω_{set}, the area under the curve is constant for different ω_{set}.

Since Eq. (2d) includes both laminar and turbulent regimes, we discuss the effect of these regimes on the centrifugal emulsification process. To compare the laminar and turbulent regimes, we focus on Eq. (4b). For the same value of H_1, h_{air}, d_1 and d_n, we find that $U_0 \propto \omega_{\text{set}}^2$ in the laminar regime whereas $U_0 \propto \omega_{\text{set}}^{\frac{8}{7}}$ in the turbulent regime. Since U_0 directly influences U_{exit} (see Eqs. (2a) and (4a)), the laminar regime is more efficient in increasing shear rates with an increase in ω_{set}. However, an increase in ω_{set} implies an increase in U_{exit}, which in turn increases the Re and modifies the regime from laminar to turbulent.

Following Eqs. (4a, 4b), d_1 can be increased to minimize the unsteady behavior of U_{exit}. This is the rationale for a double stage device that has an additional reservoir of a larger diameter d_2 (see Fig. 1c). For this case we now redefine $H = h_n + h_1 + h_2$ and $h_{\text{air}}(t)$ as the height of air column in the double-stage reservoir. For this double-stage device, Eqs. (4a), remain otherwise identical except that d_1 is replaced by d_2. We integrate the modified equations for $0 \leqslant t \leqslant t_f$ such that $h_{\text{air}}(t_f) = h_1 + h_2$.

One of the important parameters that characterizes a homogenizing device is the power density ε, *i.e.* energy per unit mass per unit time. ε is estimated as [54]

$$\varepsilon = (cU_{\text{exit}}(t))^3 d_n^{-1}, \tag{5}$$

where c is a constant with $c = \mathcal{O}(1)$ [54,55]. Physically, c represents the level of turbulence in the system [56,57]. Eq. (5) shows that ε is a function of time and thus we define an average shear rate ε_{av} as

$$\varepsilon_{\text{av}} = \frac{\int_0^{t_f} \varepsilon U_{\text{exit}} dt}{\int_0^{t_f} U_{\text{exit}} dt}. \tag{6}$$

Assuming $c = 0.2$ [55–58], we plot the variation of ε_{av} with ω_{set} and d_n in Fig. 2d and e. We note that trends will remain the same even if we choose a different value of c. The results indicate that the double stage device is superior in homogenization as compared to the single stage device due to the higher average shear rate imparted on the emulsion. We note that the kink in the variation of ε_{av} with ω_{set} for the double stage device is due to the transition from laminar to turbulent regime, which leads to a less efficient homogenization process, as discussed above. To clarify, the kink is more apparent in the double stage process because the process is less time-dependent (Fig. 2b and c) and thus the transition from laminar to turbulent flow conditions is better observed in ε_{av}. Moreover, we learn that for high ω_{set}, further increase in ω_{set} has little effect on ε_{av}. Physically, this occurs because the increase in the maximum magnitude of U_{exit} is compensated by a faster consumption of the liquid processed. We observe a similar behavior for d_n. In fact, the results show that a decrease in d_n beyond an optimum value can even reduce ε_{av}.

Overall, we find that our homogenizer is able to provide $\varepsilon_{\text{av}} = \mathcal{O}(10^5)$ W/kg, even with only a single stage. This is comparable to the performance achieved using classical commercial homogenizer designs producing similar final emulsion droplet sizes ($d_p \approx 10$—$20\ \mu$m) to us, as reported in the literature [9,10,24–26].

Emulsions typically follow a Newtonian behavior for volume fraction of $\phi < 0.6$ [59] and therefore, we expect our model to hold for volume fractions up to $\phi \approx 0.6$. For larger values of ϕ, *i.e.* $\phi > 0.6$, emulsions follow a shear thinning behavior [59], and the model needs to be corrected. We note that Eqs. ((2a)–(2c)), are independent of the rheological properties of the emulsions, and only Eq. (2d) and the definition of Re would need to be appropriately modified for a non-Newtonian fluid. Physically, a shear thinning fluid would only improve the homogenization process and thus a simplistic model with zero-shear viscosity might serve as a good first order approximation to predict a lower bound of ε_{av}.

4. Experimental observations during emulsification

To demonstrate the capability of the homogenizer, we prepared emulsions consisting of small-sized droplets by centrifuging a mixture of oil, water, and surfactant (as described in Section 2.2) through the device. Though the results presented here are for an emulsification application, the trends observed are also relevant to other homogenizer applications such as cell lysis (as is demonstrated later in this paper), mixing of high-viscosity fluids, and breakup of aggregates [60,61].

Using CHD, we homogenized 1% oil-in-water pre-emulsion with droplet size $d_p \approx 10^2\ \mu$m and approximately 60% polydispersed for 4 different values of ω_{set}. We conducted a pass-by-pass analysis of CHD, *i.e.* we investigated the emulsion before it was re-introduced in the device. Fig. 3a and b show that beyond one pass ($N = 1$), the average droplet size d_p and polydispersity c_v (ratio of d_p standard deviation and mean) are relatively insensitive to N. We note that using the double stage CHD yields emulsions with smaller size and narrower distributions. Similarly, Fig. 3c and d show that d_p decreases with increasing ω_{set} for both the single and the double stage CHD, but that c_v is relatively insen-

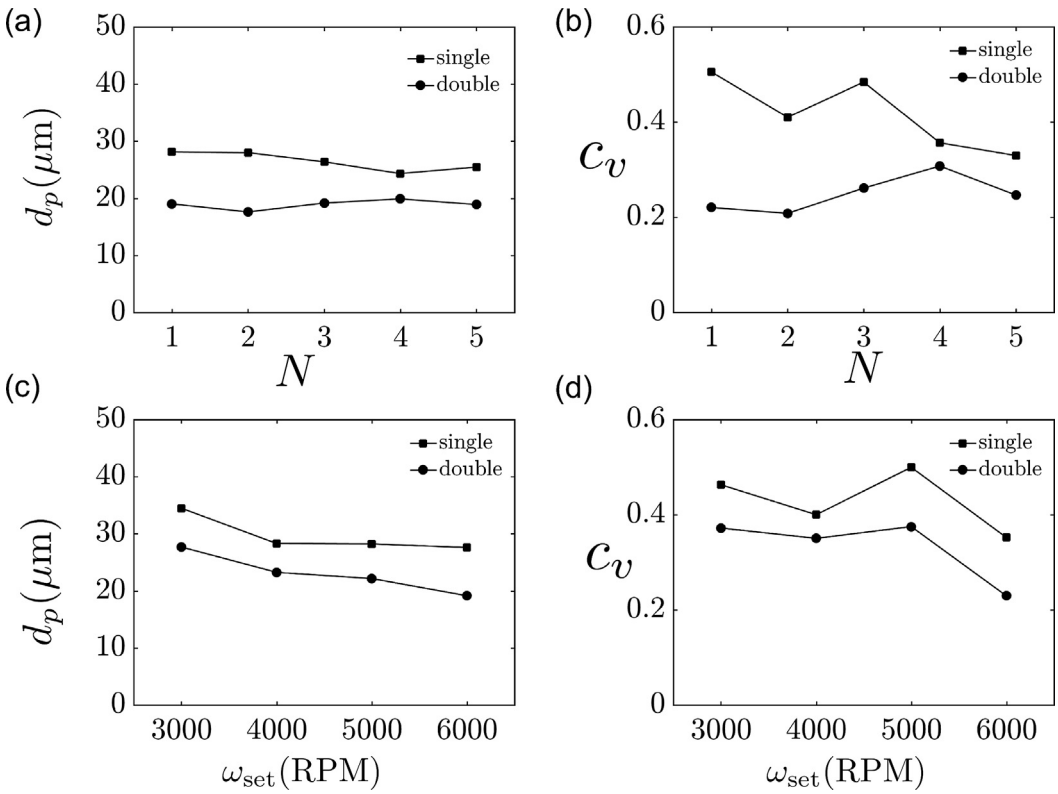

Fig. 3. Comparison between single stage and double stage emulsification. (a) Variation of average droplet size d_p and (b) polydispersity c_v with number of passes N for single stage and double stage devices. $d_n = 108$ μm, $\omega_{set} = 6000$ RPM, and oil viscosity $\mu_d = 5$ cP. Variation of (c) d_p and (d) c_v with ω_{set} for both types of devices. $N = 5$, $d_n = 108$ μm, and $\mu_d = 5$ cP.

sitive to ω_{set}. Furthermore, the double stage CHD consistently produces smaller droplet sizes with narrower size distributions (see Fig. 3d).

To interpret the experimental data, we invoke the following relation for equilibrium droplet size ($N \to \infty$), as proposed by Gupta et al. [7,27,28]:

$$\mathrm{We} = c_1 + c_2 \mathrm{Oh}^{0.4}, \tag{7a}$$

$$\mathrm{We} = \frac{\rho_c \varepsilon^{2/3} d_p^{5/3}}{\sigma}, \tag{7b}$$

$$\mathrm{Oh} = \frac{\mu_d}{\sqrt{\rho_d \sigma d_p}}, \tag{7c}$$

where We is the Weber number that quantifies the ratio of applied stress to the interfacial stress, Oh is the Ohnesorge number that quantified the ratio of internal viscous stress of the droplet to interfacial and inertial stress, σ is the interfacial tension between oil and water phases, ρ_d and μ_d are droplet density and viscosity, and c_1 and c_2 are constants, generally obtained from fitting. For $\mathrm{Oh} \ll 1$, we obtain $\mathrm{We} = c_1$, or Hinze's prediction for emulsions with $d_p \approx 1$ mm [62]. For $\mathrm{Oh} \gg 1$, we obtain $\mathrm{We} = c_2\,\mathrm{Oh}^{0.4}$, the relation proposed by Gupta et al. for nanoemulsions where $d_p \approx 100$ nm. Since our d_p lies in the middle of the two limits, we use a combination of both the limits.

First, we discuss the effect of N. We find that d_p is insensitive to N. This is expected since in our system $\mathrm{Oh} < 1$, suggesting a relatively efficient droplet breakup [28]. Moreover, within one pass ($t = 180$ s), almost the entire volume is processed, see Fig. 2b and c. Next, we compare the mean d_p between the single-stage device and the double-stage device. Eqs. (7a, 7b) suggest that irrespective of Oh, $d_p \propto \varepsilon^{-2/5}$. Based on our calculations in Fig. 2d, we find that ε_{av} for the double stage device is about 25 times that of the single stage device. Accordingly, d_p for the double stage device is predicted to be about 30% of d_p for the single stage device. Similarly, an increase of ω_{set} from 3000 to 6000 RPM suggests a reduction to about 25% in d_p. However, experimentally, we observe that d_p for the double stage device is about 70% of d_p for the single stage device, and the d_p for 6000 RPM is about 70% of d_p for 3000 RPM. We argue that this discrepancy occurs due to the assumption made in estimating U_{exit} of fully developed flow that leads to an over prediction of sensitivity with ω_{set}, especially for the large nozzle diameter cases where the ratio of nozzle length to diameter is not very large. However, the experimental trends are in qualitative agreement with our model. We note that c_v is always lower for the double stage device (Fig. 3b and d). This is explained through a more uniform U_{exit} for a double stage device (Fig. 2b and c).

We also examine the effect of d_n on d_p and c_v (see Fig. 4c and d). We find that a larger d_n leads to a slightly larger d_p, despite the relatively weak dependence of ε_{av} on d_n when compared with the single stage device. The effect of d_n is non-monotonic due the nonlinear dependence of ε_{av} (see Fig. 2e). Interestingly, we note that the experimental results are qualitatively consistent with our prediction for single stage device where ε decreases with increase in d_n. The dependence of d_p on d_n places a practical limitation on the smallest droplets CHD can prepare due to availability of small diameter needles. For a given centrifugal speed d_n strongly influences the ε_{av}, and consequently droplet size. Next, we study the influence of the dispersed phase viscosity μ_d on d_p; see Fig. 4a and b. We observe that d_p is larger for a larger μ_d. This trend is explained through the effect of Oh on d_p (see Eqs. 7a, 7b). A larger Oh leads to a higher d_p. However, a quantitative comparison is not possible since our experimental data is insufficient to reliably fit

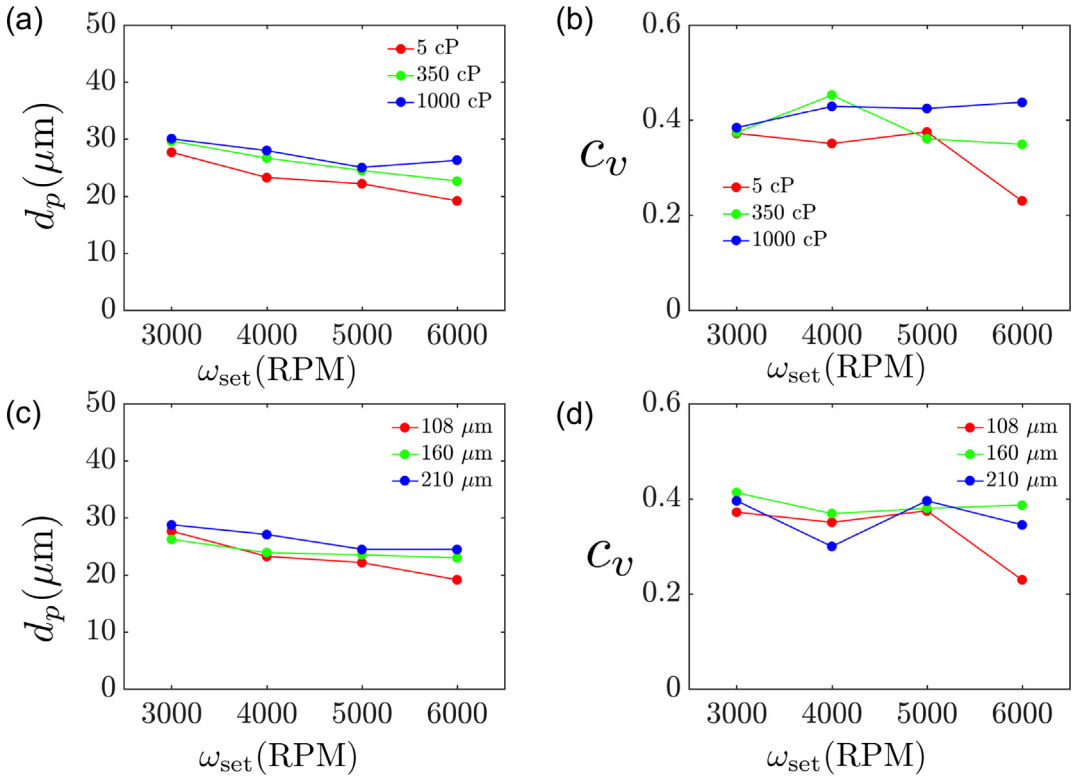

Fig. 4. Effect of nozzle diameter μ_d and droplet viscosity d_n. The results presented here are for a double stage device. Variation of (a) d_p and (b) c_v with ω_{set} for different μ_d. $N = 5$ and $d_n = 108$ μm. Variation of (c) average droplet size d_p and (d) polydispersity c_v with ω_{set} for different d_n. $N = 5$ and $\mu_d = 5$ cP.

values of c_1 and c_2. The polydispersity c_v of the resulting emulsion displays no clear trend with either d_n or μ_d.

As opposed to microfluidic devices that utilize low Reynolds number multiphase flows driven by centrifugal forces[45], our CHD operates at significantly higher Reynolds numbers, in a turbulent flow regime. Consequently, it can process 10 mL fluid volumes within 30 s i.e. approximately 0.3 mL/s at Reynolds numbers in excess of 2000. Operation at high flow rates compromises however the ability to produce monodisperse droplets. The lowest polydispersity achieved in our experiments is 20%.

5. Application to mechanical cell lysis

As a further presentation of the utility of CHD, the mechanical lysis of cells is demonstrated in Fig. 5. Lysis is the process of removing contents of a cell, for example DNA, certain proteins, or organelles, through rupture of the cell's outer lipid membrane. This may be desired so that these contents are available for use in subsequent processes or analysis, such as DNA sequencing [63]. Lysis is often achieved through the introduction of chemicals, such as a detergent-based buffer solution, but has also been performed mechanically [64]. Mechanical lysis has the advantage of avoiding contamination of the culture sample, but has previously required complex manufactured geometries or equipment [65]. The presently considered centrifugal homogenization device is constructed of simple, readily available, and low-cost components.

In the cell lysis experiments detailed in Section 2.3, portions of the cell culture measuring 10 mL were placed in the centrifugal homogenization device and spun at 3000, 6000, or 9000 RPM for two minutes. The resulting homogenized culture was then reintroduced into the CHD and the process repeated ten times.

To quantify the extent of cell lysis, the concentration of protein released by the lysed cells into solution was measured using UV absorption spectroscopy at 280 nm wavelength. Aromatic amino acids such as tryptophan and tyrosine have absorption peaks at this wavelength [66], and are major components of proteins found in eukaryotic cells such as mpkCCD. During homogenization, the cells sediment to the bottom of the centrifuge tube, such that post-homogenization it was possible to retrieve a cell-free sample from the upper part of the tube, for subsequent UV absorption testing. Proteins which have been released from the cells due to mechanical lysis remain in solution as their sedimentation coefficient is several orders of magnitude lower. The 280 nm wavelength absorption was measured for each homogenized sample, and normalized with the absorption value of the original cell culture prior to the homogenization step. Hence the absorption values lie in the range $\in [0, 1]$, where 0 represents the value for medium containing no cells and 1 represents the value for the cell culture containing cells at the original culture density prior to homogenization. The homogenization and UV absorption measurements were performed four times at each centrifuge rotation speed. These results (shown in Fig. 5) indicate that the centrifugal homogenization is successful at releasing a significant portion of the protein from the cells into solution. With increasing rotation speed, the proportion of protein released also increases. At 9000 RPM, the value of the normalized absorption is 0.90 ± 0.08, indicating that almost all protein content initially in the mpkCCD cells is suspended in the medium, and therefore our procedure leads to the successful lysis of almost all cells initially in the culture.

Before homogenization and after homogenization, small samples of culture were imaged under an inverted microscope at 40× magnification to observe the physical effect of homogenization on the cells directly. Images of the unhomogenized sample and the sample after homogenization at 9000 RPM are given in Fig. 5b and c. Although some cells maintain their structural integrity through the homogenization process, the presence of cell debris post-homogenization confirms that lysis has occurred.

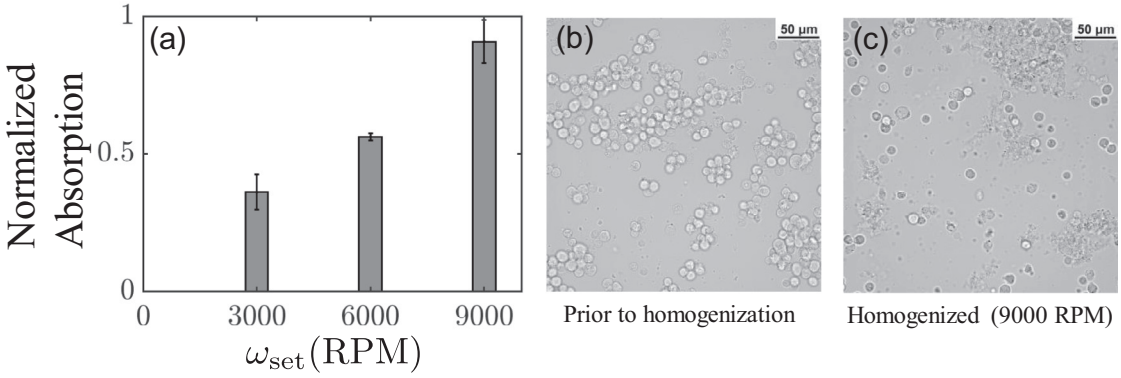

Fig. 5. (a) Absorption of UV at 280 nm wavelength by samples of mpkCCD cells homogenized at various rotation speeds. (b,c) Light microscopy images at 40× magnification of mpkCCD cells (b) before, and (c) after homogenization at 9000 RPM.

6. Conclusion

In this study, the hydrodynamic mechanisms governing centrifugal homogenization were elucidated, and a theoretical model guiding future applications of centrifugal homogenization is developed. The theoretical modelling covering both the laminar and turbulent flow regimes supported by experiments is a novel addition to this field. Guided by our theoretical developments, we have detailed the design of a low-cost centrifugal homogenizer device (CHD), constructed using only off-the-shelf parts commonly available in a standard laboratory environment. We have demonstrated successful application of this CHD in both emulsification and mechanical cell lysis.

The dependence of emulsion droplet size on centrifugal speed, dispersed phase viscosity, and nozzle size was examined, and showed qualitative agreement between the experiments and our theoretical modelling. Consistent with our modelling, we showed that double stage CHD improves homogenization performance, primarily through enforcing more constant nozzle velocities throughout operation compared to single stage CHD. Furthermore our device design is able to achieve a power density, $\varepsilon_{av} = \mathcal{O}(10^5)$ W/kg, which is comparable to what has been reported in the literature [9,10,24–26] for commercial homogenizers but with much greater throughput when compared to microfluidic emulsification approaches leveraging centrifugal forces [45].

Since we are able to achieve reasonably high power densities, our method may provide a new route to mix high viscosity fluids and breakup of aggregates. In future, we will pursue further improvement and optimization in the design of CHD through additive manufacturing. Of particular interest is the potential for application in fast lysis of different cell types including the more challenging problem of bacterial lysis.

Appendix A. Supplementary material

Supplementary data associated with this article can be found, in the online version, at https://doi.org/10.1016/j.jcis.2019.03.036.

References

[1] F. Leal-Calderon, V. Schmitt, J. Bibette, Emulsion Scince: Basic Princibles, Springer, 2007.
[2] R. Aveyard, B.P. Binks, J.H. Clint, Emulsions stabilised solely by colloidal particles, Adv. Colloid Interface Sci. 100–102 (2003) 503–546.
[3] A. Huerre, M. De Corato, V. Garbin, Dynamic capillary assembly of colloids at interfaces with 10,000g accelerations, Nat. Commun. 9 (1) (2018) 3620.
[4] A. Imhof, D.J. Pine, Ordered macroporous materials by emulsion templating, Nature 948 (1997) EP–.
[5] S.D. Kimmins, N.R. Cameron, Functional porous polymers by emulsion templating: recent advances, Adv. Funct. Mater. 21(2), (2011), 211–225.
[6] Stability of nonaqueous emulsions, J. Colloid Interface Sci. 192 (2) (1997) 368–374.
[7] A. Gupta, H.B. Eral, T.A. Hatton, P.S. Doyle, Nanoemulsions: formation, properties and applications, Soft Matter 12 (2016) 2826–2841.
[8] C. Solans, P. Izquierdo, J. Nolla, N. Azemar, M. Garcia-Celma, Nano-emulsions, Curr. Opin. Colloid Interface Sci. 10 (34) (2005) 102–110.
[9] J. Davies, Drop sizes of emulsions related to turbulent energy dissipation rates, Chem. Eng. Sci. 40 (5) (1985) 839–842.
[10] J. Davies, A physical interpretation of drop sizes in homogenizers and agitated tanks, including the dispersion of viscous oils, Chem. Eng. Sci. 42 (7) (1987) 1671–1676.
[11] J. Floury, J. Bellettre, J. Legrand, A. Desrumaux, Analysis of a new type of high pressure homogeniser. A study of the flow pattern, Chem. Eng. Sci. 59 (4) (2004) 843–853.
[12] J. Floury, J. Legrand, A. Desrumaux, Analysis of a new type of high pressure homogeniser. Part b. Study of droplet break-up and recoalescence phenomena, Chem. Eng. Sci. 59 (6) (2004) 1285–1294.
[13] Analysis of a new type of high pressure homogeniser. A study of the flow pattern, Chem. Eng. Sci. 59(4) (2004) 843–853.
[14] K. Meleson, S. Graves, T.G. Mason, Formation of concentrated nanoemulsions by extreme shear, Soft Mater. 2 (2–3) (2004) 109–123.
[15] K.P. Velikov, E. Pelan, Colloidal delivery systems for micronutrients and nutraceuticals, Soft Matter 4 (2008) 1964–1980.
[16] H.B. Eral, M. O'Mahony, R. Shaw, B.L. Trout, A.S. Myerson, P.S. Doyle, Composite hydrogels laden with crystalline active pharmaceutical ingredients of controlled size and loading, Chem. Mater. 26 (21) (2014) 6213–6220.
[17] H.B. Eral, V. López-Mejías, M. O'Mahony, B.L. Trout, A.S. Myerson, P.S. Doyle, Biocompatible alginate microgel particles as heteronucleants and encapsulating vehicles for hydrophilic and hydrophobic drugs, Cryst. Growth Des. 14 (4) (2014) 2073–2082.
[18] N. Anton, T.F. Vandamme, Nano-emulsions and micro-emulsions: clarifications of the critical differences, Pharmaceut. Res. 28 (5) (2011) 978–985.
[19] D.J. McClements, Edible nanoemulsions: fabrication, properties, and functional performance, Soft Matter 7 (6) (2011) 2297–2316.
[20] C. Qian, D.J. McClements, Formation of nanoemulsions stabilized by model food-grade emulsifiers using high-pressure homogenization: factors affecting particle size, Food Hydrocoll. 25 (5) (2011) 1000–1008.
[21] O. Sonneville-Aubrun, J.-T. Simonnet, F. L'alloret, Nanoemulsions: a new vehicle for skincare products, Adv. Colloid Interface Sci. 108 (2004) 145–149.
[22] H.Z. An, H.B. Eral, L. Chen, M.B. Chen, P.S. Doyle, Synthesis of colloidal microgels using oxygen-controlled flow lithography, Soft Matter 10 (2014) 7595–7605.
[23] T. Delmas, H. Piraux, A.-C. Couffin, I. Texier, F. Vinet, P. Poulin, M.E. Cates, J. Bibette, How to prepare and stabilize very small nanoemulsions, Langmuir 27 (5) (2011) 1683–1692.
[24] N. Vankova, S. Tcholakova, N.D. Denkov, I.B. Ivanov, V.D. Vulchev, T. Danner, Emulsification in turbulent flow: 1. Mean and maximum drop diameters in inertial and viscous regimes, J. Colloid Interface Sci. 312 (2) (2007) 363–380.
[25] N. Vankova, S. Tcholakova, N.D. Denkov, V.D. Vulchev, T. Danner, Emulsification in turbulent flow: 2. Breakage rate constants, J. Colloid Interface Sci. 313 (2) (2007) 612–629.
[26] S. Tcholakova, N. Vankova, N.D. Denkov, T. Danner, Emulsification in turbulent flow: 3. Daughter drop-size distribution, J. Colloid Interface Sci. 310 (2) (2007) 570–589.
[27] A. Gupta, H.B. Eral, T.A. Hatton, P.S. Doyle, Controlling and predicting droplet size of nanoemulsions: scaling relations with experimental validation, Soft Matter 12 (2016) 1452–1458.
[28] A. Gupta, V. Narsimhan, T.A. Hatton, P.S. Doyle, Kinetics of the change in droplet size during nanoemulsion formation, Langmuir 32 (44) (2016) 11551–11559.
[29] K. Meleson, S. Graves, T.G. Mason, Formation of concentrated nanoemulsions by extreme shear, Soft Mater. 2 (2–3) (2004) 109–123.

[30] T. Gothsch, J.H. Finke, S. Beinert, C. Lesche, J. Schur, S. Buettgenbach, C. Müller-Goymann, A. Kwade, Effect of microchannel geometry on high-pressure dispersion and emulsification, Chem. Eng. Technol. 34 (3) (2011) 335–343.
[31] R. Seemann, M. Brinkmann, T. Pfohl, S. Herminghaus, Droplet based microfluidics, Rep. Prog. Phys. 75(1), (2011), 016601.
[32] J.T. Nevill, R. Cooper, M. Dueck, D.N. Breslauer, L.P. Lee, Integrated microfluidic cell culture and lysis on a chip, Lab Chip 7 (2007) 1689–1695.
[33] J. Kim, J.W. Hong, D.P. Kim, J.H. Shin, I. Park, Nanowire-integrated microfluidic devices for facile and reagent-free mechanical cell lysis, Lab Chip 12 (2012) 2914–2921.
[34] Grinding lysis (gl): a microfluidic device for sample enrichment and mechanical lysis in one, Sens. Actuat. B: Chem. 258 (2018) 148–155.
[35] D.D. Carlo, K.-H. Jeong, L.P. Lee, Reagentless mechanical cell lysis by nanoscale barbs in microchannels for sample preparation, Lab Chip 3 (2003) 287–291.
[36] A novel, compact disk-like centrifugal microfluidics system for cell lysis and sample homogenization, Colloids Surf. B: Biointerf. 58(1) (2007) 44–51 (Supramolecular Chemistry Applied to Interfaces).
[37] M.-J. Seo, J.-C. Yoo, Lab-on-a-disc platform for automated chemical cell lysis, Sensors 18 (3) (2018) 687.
[38] M. Shimoda, H. Miyamae, K. Nishiyama, T. Yuasa, S. Noma, N. Igura, Swirl-flow membrane emulsification for high throughput of dispersed phase flux through shirasu porous glass (spg) membrane, J. Chem. Eng. Japan 44 (1) (2011) 1–6.
[39] H.B. Eral, E.R. Safai, B. Keshavarz, J.J. Kim, J. Lee, P.S. Doyle, Governing principles of alginate microparticle synthesis with centrifugal forces, Langmuir 32 (28) (2016) 7198–7209.
[40] A. Gupta, A.Z.M. Badruddoza, P.S. Doyle, A general route for nanoemulsion synthesis using low-energy methods at constant temperature, Langmuir 33 (28) (2017) 7118–7123.
[41] A.Z.M. Badruddoza, A. Gupta, A.S. Myerson, B.L. Trout, P.S. Doyle, Low energy nanoemulsions as templates for the formulation of hydrophobic drugs, Adv. Therapeut. 1 (2018) 1700020.
[42] S. Haeberle, T. Brenner, R. Zengerle, J. Ducree, Centrifugal extraction of plasma from whole blood on a rotating disk, Lab Chip 6 (2006) 776–781.
[43] M. Grumann, A. Geipel, L. Riegger, R. Zengerle, J. Ducree, Batch-mode mixing on centrifugal microfluidic platforms, Lab Chip 5 (2005) 560–565.
[44] M. La, S.J. Park, H.W. Kim, J.J. Park, K.T. Ahn, S.M. Ryew, D.S. Kim, A centrifugal force-based serpentine micromixer (csm) on a plastic lab-on-a-disk for biochemical assays, Microfluid. Nanofluid. 15 (1) (2013) 87–98.
[45] F. Schuler, F. Schwemmer, M. Trotter, S. Wadle, R. Zengerle, F. von Stetten, N. Paust, Centrifugal step emulsification applied for absolute quantification of nucleic acids by digital droplet RPA, Lab Chip 15 (2015) 2759–2766.
[46] F. Schuler, C. Siber, S. Hin, S. Wadle, N. Paust, R. Zengerle, F. von Stetten, Digital droplet lamp as a microfluidic app on standard laboratory devices, Anal. Meth. 8 (2016) 2750–2755.
[47] F. Schuler, N. Paust, R. Zengerle, F. Von Stetten, Centrifugal step emulsification can produce water in oil emulsions with extremely high internal volume fractions, J.
[48] X. Mao, T.J. Huang, Microfluidic diagnostics for the developing world, Lab Chip 12 (2012) 1412–1416.
[49] A.W. Martinez, S.T. Phillips, G.M. Whitesides, E. Carrilho, Diagnostics for the developing world: microfluidic paper-based analytical devices, Anal. Chem. 82 (1) (2010) 3–10.
[50] F. Salamanca-Buentello, D.L. Persad, E.B. Court, D.K. Martin, A.S. Daar, P.A. Singer, Nanotechnology and the developing world, PLOS Med. 2 (5) (2005) 383–386.
[51] D.C.H. Burgess, J. Wasserman, C.A. Dahl, Global health diagnostics, Nature 444 (1s) (2006) 1.
[52] N. Ahmed, D. Sukovich, A.R. Abate, Operation of droplet-microfluidic devices with a lab centrifuge, Micromachines 7 (9) (2016) 161.
[53] J.-P. Duong Van Huyen, M. Bens, A. Vandewalle, Differential effects of aldosterone and vasopressin on chloride fluxes in transimmortalized mouse cortical collecting duct cells, J. Membr. Biol. 164 (1) (1998) 79–90.
[54] W.M. Deen, Introduction to Chemical Engineering Fluid Mechanics, Cambridge University Press, 2016.
[55] A. Håkansson, L. Fuchs, F. Innings, J. Revstedt, C. Trägårdh, B. Bergenståhl, High resolution experimental measurement of turbulent flow field in a high pressure homogenizer model and its implications on turbulent drop fragmentation, Chem. Eng. Sci. 66 (8) (2011) 1790–1801.
[56] F. Innings, C. Trägårdh, Analysis of the flow field in a high-pressure homogenizer, Exp. Therm. Fluid Sci. 32 (2) (2007) 345–354.
[57] A. Håkansson, C. Trägårdh, B. Bergenståhl, Dynamic simulation of emulsion formation in a high pressure homogenizer, Chem. Eng. Sci. 64 (12) (2009) 2915–2925.
[58] K.-H. Mohr, High-pressure homogenization. Part i. Liquid-liquid dispersion in turbulence fields of high energy density, J. Food Eng. 6 (3) (1987) 177–186.
[59] R. Pal, Shear viscosity behavior of emulsions of two immiscible liquids, J. Colloid Interface Sci. 225 (2) (2000) 359–366.
[60] P. Oresta, A. Prosperetti, Effects of particle settling on rayleigh-bénard convection, Phys. Rev. E 87, (2013), 063014.
[61] I.M. Mazzitelli, F. Fornarelli, A.S. Lanotte, P. Oresta, Pair and multi-particle dispersion in numerical simulations of convective boundary layer turbulence, Phys. Fluids 26 (5) (2014) 055110.
[62] J.O. Hinze, Fundamentals of the hydrodynamic mechanism of splitting in dispersion processes, AIChE J. 1 (3) (1955) 289–295.
[63] A. Kashyap, J. Autebert, E. Delamarche, G.V. Kaigala, Selective local lysis and sampling of live cells for nucleic acid analysis using a microfluidic probe, Sci. Rep. 6 (2016) 29579.
[64] M. Shehadul Islam, A. Aryasomayajula, P.R. Selvaganapathy, A review on macroscale and microscale cell lysis methods, Micromachines 8 (3) (2017) 83.
[65] L. Nan, Z. Jiang, X. Wei, Emerging microfluidic devices for cell lysis: a review, Lab Chip 14 (2014) 1060–1073.
[66] G. Beaven, E. Holiday, Ultraviolet absorption spectra of proteins and amino acids, Advances in Protein Chemistry, vol. 7, Academic Press, 1952, pp. 319–386.